Hindawi
Geofluids
Volume 2023, Article ID 4030804, 13 pages
https://doi.org/10.1155/2023/4030804

Research Article

Porothermoelastic Response of a Borehole in Fluid-Saturated Medium Subjected to Thermal Osmosis Effect

Hai Lin,[1,2] **Jingen Deng**,[1] **Xiaocheng Zhang**,[2] **and Jiajia Gao**[3]

[1]*State Key Laboratory of Petroleum Resource & Prospecting, China University of Petroleum, Beijing 102249, China*
[2]*CNOOC China Limited, Tianjin Branch, Tianjin 300459, China*
[3]*Petroleum Engineering School, Southwest Petroleum University, Chengdu 610500, China*

Correspondence should be addressed to Jingen Deng; dengjingen@126.com

Received 19 October 2021; Revised 1 March 2022; Accepted 6 April 2023; Published 22 May 2023

Academic Editor: Basim Abu-Jdayil

With the thermo-hydro-mechanical coupling process considered, this paper derives a set of analytical porothermoelastic solutions to field variables including the stress, displacement, and pore pressure fields to evaluate the wellbore stability around a vertical borehole drilled through an isotropic porous rock. The thermal effect on the wellbore stability of the low-permeability saturated rock also introduces the thermal osmosis term. The wellbore problem is decomposed into axisymmetric and deviatoric loading cases considering the borehole subjected to a nonhydrostatic stress field. It obtains the time-dependent distributions of field variables by performing the inversion technique for Laplace transforms to the porothermoelastic solutions in the Laplace domain. The results suggest that the thermal osmosis effect should not be neglected on the premise that a lower permeability porous rock is characterized by the substantially large thermal osmotic coefficient and the small thermal diffusivity values. The case that the thermal osmosis effect reduces the undrained loading effect leads to the decrease of the mean shear stress that is determined by the effective maximum and minimum stress around a borehole, since, and accordingly contributes to the wellbore stability to resist the shear failure.

1. Introduction

When the deep-water and unconventional oil and gas resources are drilled in the high-temperature and high-pressure (HTHP) block, drilling a borehole experiences a large temperature difference between the drilling mud and formation fluid. The coupled thermo-hydraulic-mechanical (THM) effect of fluid-saturated porous media inevitably implicates time-dependent wellbore instability issues, since the thermal loading progressively reestablishes the induced stresses and pore pressure around a wellbore [1–23]. Moreover, the poroelastic effect associated with undrained loading [24, 25] also contributes to the remodifications of field variables after instantaneously drilling a borehole, especially for low-permeability porous medium.

Detournay and Cheng [24] adopted the field variables including displacement, stress, and pore pressure around a borehole to discuss the coupled hydromechanical effect. Three different modes are used to obtain the complete solution of field variables. Mode 1 is a classical elastic case and not related to the coupled issue. The content of mode 2 is purely pressure radial (or axisymmetric) diffusion around a borehole and is attributed to the partially coupled process. It means that the pore pressure induces the occurrence of stresses and displacement whereas the opposite process does not take place. Mode 3 is a fully coupled process. The pore pressure perturbation leads to the induced stresses and solid displacements; accordingly, the stress perturbation also induces a pore pressure built-up regime near the borehole wall due to the undrained loading. The undrained loading gives rise to the occurrence of the excess pore pressure case for low-permeability porous rock. This is because that the pore fluid is not allowed to have enough time to escape the current pore space delimited by the solid pore wall, when the undrained loading is quickly applied to the porous rock. The pore fluid naturally suffers the undrained loading effect and causes an excess pore pressure to generate in the pore-space. It refers the excess pore pressure case to as an

undrained state subjected by the low-permeability porous rock. This phenomenon exactly explains the poroelastic effect to embody the coupled solid deformation and fluid flow in the porous medium.

The thermal effect introduced by the coupled THM process is embodied in the radial diffusion problem and induces pore pressure and stresses around a wellbore. That is to say, the thermal effect alone appears in a developed mode 2 that differs from the aforementioned study of Detournay and Cheng [24] and renders the pore pressure diffusion to depend on the temperature variation [1–23]. Besides, the thermal osmosis effect is observed by conducting the experiment [26–31] or discussed in studies [6–8, 19–23].

Thermal osmosis effect accounts for the contribution of temperature gradient on the fluid flux and becomes significant for expected temperature gradients in the case of the clay barriers of waste disposal with extremely low hydraulic conductivity (10^{-10} and 10^{-14} m/s) [6, 29]. The thermal osmosis effect resembles the Sorêt effect in a chemical solution that causes a chemical flux proportional to the temperature gradient [2]. Besides, the indirect thermal osmosis flow may significantly contribute to mass transfer induced in semi-impermeable clays compared to the direct Darcian flow [28]. The studies [19–23] further support the viewpoint of Ghassemi and Diek [8]. Namely, a case associated with a substantially large thermoosmotic coefficient and a larger temperature gradient significantly facilitates the thermal osmosis effect to modify the change in pore pressure near a borehole. Both positive and negative values of the thermal osmosis coefficient K^{T} are possibly observed in rocks [26]. In the case of $K^{\mathrm{T}} < 0$, the osmotic flow direction is from warmer to cooler, while in the case of $K^{\mathrm{T}} > 0$, the flow is from cooler to warmer [31]. Nevertheless, the flow in both directions in laboratory tests is using compacted clays [27]. The absolute value of thermal osmotic coefficient K^{T} ranges from 10^{-14} to $10^{-10}\,\mathrm{m}^2/(\mathrm{s}\cdot\mathrm{K})$ for different porous media [30].

Several relevant studies [2, 6, 7, 9, 10, 15, 16] neglected the nonlinear convective heat transfer term that couples temperature with pore pressure to obtain the engineering-oriented analytical linear-porothermoelastic solutions. However, this partially decoupled operation alone holds for low-permeability rocks [9]. Besides, the abovementioned porothermoelastic analytical solutions neglect the thermal osmosis effect [3–5, 10–16].

The present paper newly formulates coupled porothermoelastic solution with thermal osmosis for a vertical borehole in a nonhydrostatic stress field. Accordingly, the results from this paper could provide theoretical guidance for effectively dealing with the complicated issues during drilling through the low permeability and low porosity formation.

2. General Formulations

The governing equations in the present model are presented as follows.

2.1. Constitutive Equations. Introducing the thermal effect into the work of Detournay and Cheng [32] or extending the study of Zimmerman [33], the constitutive Equations (1) and (2) take the following forms to accurately show the coupled thermo-hydro-mechanical behavior when the isotropic fluid saturated porous medium deforms in the elastic state. Besides, the constitutive Equations (1) and (2) are written as that the positive stress denotes compression in line with the rock mechanics convention.

$$\sigma_{ij} = 2G\varepsilon_{ij} + \lambda\varepsilon + \alpha p\delta_{ij} + \beta^s T\delta_{ij}, \tag{1}$$

$$\zeta = -\alpha\varepsilon + \frac{p}{M} - \beta^{fs}T. \tag{2}$$

The abovementioned equations include total stresses tensor σ_{ij}, pore pressure p, temperature variations T, strain tensor for the solid rock ε_{ij}, volumetric strain $\varepsilon = \varepsilon_{ii}$, and the variation of fluid content per unit reference volume ζ. The material constants include drained Poisson's ratio ν, rock shear modulus G, and the Lame constant λ defined by $\lambda = 2G\nu/(1-2\nu)$. δ_{ij} is the Kronecker delta. Besides, Biot coefficient α and modulus M are written as follows:

$$\alpha = 1 - \frac{K}{K_s}, \frac{1}{M} = \frac{\alpha-\phi}{K_s} + \frac{\phi}{K_f}, \tag{3}$$

where the rock bulk modulus K is defined by $3K = 2G(1+\nu)/(1-2\nu)$. K_s and K_f are the bulk modulus of solid grain and fluid, respectively. ϕ is rock intrinsic porosity.

The thermic coefficients related to solid skeleton β^s and solid-fluid β^{fs} are read as follows [11]:

$$\begin{aligned} \beta^s &= 3K\alpha^s, \\ \beta^{fs} &= 3\alpha\alpha^s + \phi\left(\alpha^f - 3\alpha^s\right), \end{aligned} \tag{4}$$

where the symbols α^s and α^f are the linear expansion coefficient for solid matrix and volumetric expansion coefficient for fluid, respectively.

2.2. Field Equations. In the case of the infinitely long borehole and constant boundary condition along the borehole axis direction, both fluid and heat flux components will disappear along the direction of the borehole axis [11]. With Equation (2) and thermal osmosis term considered into fluid flux [8], the fluid diffusive equation for weakly compressive and thermally expansible fluid reads as follows:

$$\frac{1}{M}\frac{\partial p}{\partial t} - \alpha\frac{\partial \varepsilon}{\partial t} - \beta^{fs}\frac{\partial T}{\partial t} - \kappa\nabla^2 p + K^{\mathrm{T}}\nabla^2 T = 0, \tag{5}$$

where the permeability coefficient κ is expressed as $\kappa = k/\mu$ in which k is the intrinsic permeability tensor and μ is the fluid viscosity. K^{T} denotes the thermal osmosis coefficient. The linear differential operator ∇^2 is written as follows:

$$\nabla^2 = \frac{1}{r}\frac{\partial}{\partial r}\left(r\frac{\partial}{\partial r}\right) + \frac{\partial^2}{r^2\partial\theta^2}. \quad (6)$$

Provided that the assumption of instantaneous local temperature equilibrium holds, the heat diffusive field equation takes the form of Wang and Papamichos [4]:

$$\rho_m c_m \frac{\partial T}{\partial t} - k^{\mathrm{T}}\nabla^2 T = 0, \quad (7)$$

where ρ_m and c_m, respectively, denote the total mass density and specific heat capacity, and k^{T} is the thermal conductivity of porous rock. It holds that the effect of the strain and pore pressure on the temperature is commonly ignored [23, 33] considering the strain and coupled parameters with much smaller values. Gao et al. [19] concluded that the thermal filtration effect depending on the pressure gradient Equation (6) has a weak influence on the temperature diffusion, such that it is also ignored.

3. Borehole Problem Description and the Solution

3.1. Borehole Problem Description. A circular vertical borehole is drilled in a porous rock formation subjected to a non-hydrostatic horizontal in situ stress field; see Figure 1. It is assumed that one of the three in situ principal stresses is parallel to the borehole axis, and x - and y -axes correspond to the directions of two other in situ principal stresses.

It follows that the total stresses acting on a circular boundary are given by the following:

$$\begin{aligned}\sigma_r &= \sigma_m + \sigma_d\cos 2\theta,\\ \sigma_\theta &= \sigma_m - \sigma_d\cos 2\theta,\\ \tau_{r\theta} &= -\sigma_d\sin 2\theta,\end{aligned} \quad (8)$$

with the mean stress σ_m and shear stress σ_d are, respectively, defined by $\sigma_m = (\sigma_H + \sigma_h)/2$ and $\sigma_d = (\sigma_H - \sigma_h)/2$, in which the symbols σ_H and σ_h, respectively, are the maximum and minimum horizontal in situ stress.

The generalized plane strain assumption may be appropriate to extrapolate the solutions under a two-dimensional case to a general three-dimensional one, assuming that the geomechanics is characterized by geometries in which boundary conditions are constant along the direction of the infinitely long borehole axis [11]. In line with the loading decomposition scheme proposed by Abousleiman and Cui [34], this problem is disassembled into two separate resolved subproblems, since the antiplane shear stresses disappear in a vertical borehole. Two subproblems include a modified poroelastic plane strain problem (Problem I) and an elastic unaxial problem (Problem II). Finally, the principle of superposition to consider the linearity problem is employed to obtain the complete solutions.

3.2. Solution to Modified Poroelastic Plane Stain Problem. The boundary conditions including stress components, pore pressure, and temperature acting at borehole wall after instant drilling are described as for Problem I:

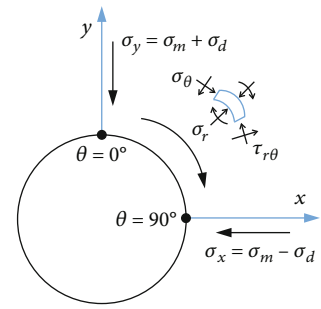

Figure 1: Schematic of borehole stress analysis.

$$\Delta\sigma_r|_{r=r_w} = p_w - [\sigma_m + \sigma_d\cos 2\theta], \quad (9a)$$

$$\Delta\tau_{r\theta}|_{r=r_w} = \sigma_d\sin 2\theta, \quad (9b)$$

$$\Delta p|_{r=r_w} = p_w - p_0, \quad (9c)$$

$$\Delta T|_{r=r_w} = T_w - T_0, \quad (9d)$$

where p_w is the wellbore pressure. T_w and T_0, respectively, are the wellbore fluid temperature and the formation temperature.

Furthermore, two separate boundary conditions at the borehole wall for each of the loading modes may be defined as follows, respectively.

(i) Axisymmetric loading:

$$\Delta\sigma_r^{(a)}\Big|_{r=r_w} = p_w - \sigma_m, \quad (10a)$$

$$\Delta\tau_{r\theta}^{(a)}\Big|_{r=r_w} = 0, \quad (10b)$$

$$\Delta p^{(a)}\Big|_{r=r_w} = p_w - p_0, \quad (10c)$$

$$\Delta T|_{r=r_w} = T_w - T_0. \quad (10d)$$

(ii) Deviatoric loading:

$$\Delta\sigma_r^{(d)}\Big|_{r=r_w} = -\sigma_d\cos 2\theta, \quad (11a)$$

$$\Delta\tau_{r\theta}^{(d)}\Big|_{r=r_w} = \sigma_d\sin 2\theta, \quad (11b)$$

$$\Delta p^{(d)}\Big|_{r=r_w} = 0. \quad (11c)$$

The boundary conditions of this problem imposed at the far field, i.e., $r \longrightarrow \infty$, are expressed as follows:

$$\begin{aligned}\sigma_r &= \sigma_m + \sigma_d \cos 2\theta,\\ \tau_{r\theta} &= -\sigma_d \sin 2\theta,\\ \sigma_z &= 2\nu\sigma_m + (1-2\nu)(\alpha p_0 + \beta^s T_0),\\ p &= p_0,\\ T &= T_0.\end{aligned} \tag{12}$$

Introducing the rotation of displacement field ω, the equilibrium equation ($\sigma_{ij'j} = 0,\ i,j \in (r,\theta)$) is written in terms of volumetric strain $\varepsilon(\varepsilon = \varepsilon_r + \varepsilon_\theta)$, variation of fluid content ζ, and temperature T:

$$\begin{aligned}&\left(\lambda + 2G + \alpha^2 M\right)\frac{\partial \varepsilon}{\partial r} - G\frac{1}{r}\frac{\partial \omega}{\partial \theta} + \alpha M\frac{\partial \zeta}{\partial r}\\ &\quad + \left(\beta^s + \alpha M\beta^{sf}\right)\frac{\partial T}{\partial r} = 0,\end{aligned} \tag{13}$$

$$\begin{aligned}&\left(\lambda + 2G + \alpha^2 M\right)\frac{1}{r}\frac{\partial \varepsilon}{\partial \theta} + G\frac{\partial \omega}{\partial r} + \alpha M\frac{1}{r}\frac{\partial \zeta}{\partial \theta}\\ &\quad + \left(\beta^s + \alpha M\beta^{sf}\right)\frac{1}{r}\frac{\partial T}{\partial \theta} = 0,\end{aligned} \tag{14}$$

where ε and ω, respectively, are defined by the following:

$$\varepsilon = \frac{1}{r}\frac{\partial}{\partial r}(ru_r) + \frac{\partial u_\theta}{r\partial \theta}, \tag{15}$$

$$\omega = -\frac{1}{r}\frac{\partial u_r}{\partial \theta} + \frac{\partial}{r\partial r}(ru_\theta). \tag{16}$$

Furthermore, the diffusive equation in terms of the variation of fluid content ζ is written as an alternative form, through combining Equations (2) and (5) with the transforms to Equations (13) and (14).

$$\frac{\partial \zeta}{\partial t} - c^*\nabla^2\left[\zeta + \left(\bar{c}^* - \frac{K^{\mathrm{T}}}{c^*}\right)T\right] = 0, \tag{17}$$

where

$$\begin{aligned}c^* &= \frac{\kappa M(\lambda + 2G)}{\alpha^2 M + (\lambda + 2G)},\\ \bar{c}^* &= \beta^{fs} - \frac{\alpha\beta^s}{\lambda + 2G}.\end{aligned} \tag{18}$$

The boundary conditions in Equations ((10a)), ((10b)), ((10c)), and ((10d)) and ((11a)), ((11b)), and ((11c)) suggest the dependence of the displacement, stress, pore pressure, and temperature upon the polar angle could be sought of which has the following form [35]:

$$\left(\tilde{\zeta}, \tilde{\varepsilon}, \tilde{u}_r, \tilde{\sigma}_r, \tilde{\sigma}_\theta, \tilde{p}, \tilde{T}\right) = \left(\tilde{Z}, \tilde{\Xi}, \tilde{U}_r, \tilde{S}_r, \tilde{S}_\theta, \tilde{P}, \tilde{H}\right)\cos m\theta, \tag{19a}$$

$$\left(\tilde{\omega}, \tilde{u}_\theta, \tilde{\tau}_{r\theta}\right) = \left(\tilde{W}, \tilde{U}_\theta, \tilde{S}_{r\theta}\right)\sin m\theta, \tag{19b}$$

with $m = 0$ for axisymmetric loading and $m = 2$ for deviatoric loading. $\tilde{Z}$, $\tilde{\Xi}$, $\tilde{U}_r$, $\tilde{U}_\theta$, $\tilde{S}_r$, $\tilde{S}_\theta$, $\tilde{S}_{r\theta}$, $\tilde{P}$, $\tilde{W}$, and $\tilde{H}$ are the functions of time t and radial distance r only. Besides, the sign"~" represents the Laplace integral transforms with respect to t and is defined by the following:

$$\tilde{f}(r,s) = \int_0^\infty f(r,t)\, e^{-st}dt, \tag{20}$$

where s is a parameter for the Laplace transform.

3.2.1. Solutions to Axisymmetric Loading

(1) Solution for Temperature. Under axis-symmetric thermal loading, Equation (8) is solved by the following initial and boundary conditions in the Laplace transformed forms:

$$\frac{\tilde{T}^{(a)}(r_w,t)}{T_m - T_0} = \frac{1}{s} \quad \frac{\tilde{T}^{(a)}(r,0)}{T_m - T_0} = 0 \quad \frac{\tilde{T}^{(a)}(\infty,t)}{T_m - T_0} = 0, \tag{21}$$

and therefore reads as follows:

$$\tilde{T}^{(a)} = m_0(s)\frac{K_0(\xi_T)}{K_0(\beta_T)}, \tag{22}$$

where

$$\begin{aligned}m_0(s) &= \frac{T_m - T_0}{s},\\ \beta_T &= r_w\sqrt{\frac{s}{c_h}},\\ \xi_T &= r\sqrt{\frac{s}{c_h}},\\ c_h &= \frac{k_T}{\rho_m c_m}.\end{aligned} \tag{23}$$

$K_n(xr)$ is the modified Bessel function of the second kind of order "n".

(2) Solutions for Pore Pressure, Radial Displacement, and Stresses. Taking into consideration of Equation (2), a simplified uncoupled pore pressure diffusion expression could be written as Equation (24) when the assumption that displacement field is irrotational in semi-infinite domain holds the following:

$$\frac{\partial p}{\partial t} - c^*\left[\nabla_r^2 p + \frac{1}{\kappa}\left(\bar{c}^*\frac{\partial T}{\partial t} - K^{\mathrm{T}}\nabla_r^2 T\right)\right] = 0, \tag{24}$$

in which

$$\nabla_r^2 = \frac{1}{r}\frac{\partial}{\partial r}\left(r\frac{\partial}{\partial r}\right). \tag{25}$$

Equation (24) may be solved by the following Laplace transformed initial and boundary conditions:

$$\frac{\tilde{p}(r_w,t)}{p_w-p_0}=\frac{1}{s}\quad \frac{\tilde{p}(r,0)}{p_w-p_0}=0\quad \frac{\tilde{p}(\infty,t)}{p_w-p_0}=0, \tag{26}$$

and thus, the solution of the pore pressure in the Laplace domain reads under axis-symmetric loading

$$\tilde{P}^{(a)}=\frac{p_w-p_0}{s}\frac{K_0(\xi)}{K_0(\beta)}-\frac{c^*}{\kappa}\left[\frac{\bar{c}^*c_T-K^{\mathrm{T}}}{c_T-c^*}m_0(s)\cdot\left(\frac{K_0(\xi)}{K_0(\beta)}-\frac{K_0(\xi_T)}{K_0(\beta_T)}\right)\right], \tag{27}$$

where

$$\xi=r\sqrt{\frac{s}{c^*}},\qquad \beta=r_w\sqrt{\frac{s}{c^*}}. \tag{28}$$

One combines Equation (1) with Equation (15) and takes into consideration the Laplace transformed boundary condition (Equation (10a)), and thus, the radial displacement and stresses for axisymmetric loading are given as follows:

$$\frac{2G\tilde{u}_r^{(a)}}{r_w}=\frac{1-2\nu}{1-\nu}\left\{n_0(s)\left[\frac{K_1(\xi)}{\beta K_0(\beta)}-\frac{r_w}{r}\frac{K_1(\beta)}{\beta K_0(\beta)}\right]+n_1(s)\left[\frac{K_1(\xi_T)}{\beta_T K_0(\beta_T)}-\frac{r_w}{r}\frac{K_1(\beta_T)}{\beta_T K_0(\beta_T)}\right]\right\}-\frac{p_w-\sigma_m}{s}\frac{r_w}{r}, \tag{29a}$$

$$\tilde{\sigma}_r^{(a)}=-\frac{1-2\nu}{1-\nu}\left\{n_0(s)\left[\frac{r_w}{r}\frac{K_1(\xi)}{\beta K_0(\beta)}-\frac{r_w^2}{r^2}\frac{K_1(\beta)}{\beta K_0(\beta)}\right]+n_1(s)\left[\frac{r_w}{r}\frac{K_1(\xi_T)}{\beta_T K_0(\beta_T)}-\frac{r_w^2}{r^2}\frac{K_1(\beta_T)}{\beta_T K_0(\beta_T)}\right]\right\}+\frac{p_w-\sigma_m}{s}\frac{r_w^2}{r^2}, \tag{29b}$$

$$\tilde{\sigma}_\theta^{(a)}=\frac{1-2\nu}{1-\nu}\left\{n_0(s)\left[\frac{r_w}{r}\frac{K_1(\xi)}{\beta K_0(\beta)}-\frac{r_w^2}{r^2}\frac{K_1(\beta)}{\beta K_0(\beta)}+\frac{K_0(\xi)}{K_0(\beta)}\right]+n_1(s)\left[\frac{r_w}{r}\frac{K_1(\xi_T)}{\beta_T K_0(\beta_T)}-\frac{r_w^2}{r^2}\frac{K_1(\beta_T)}{\beta_T K_0(\beta_T)}+\frac{K_0(\xi_T)}{K_0(\beta_T)}\right]\right\}-\frac{p_w-\sigma_m}{s}\frac{r_w^2}{r^2}, \tag{29c}$$

where

$$n_0(s)=\alpha\left[\frac{p_w-p_0}{s}-\frac{c^*}{\kappa}\frac{\bar{c}^*c_T-K^{\mathrm{T}}}{c_T-c^*}m_0(s)\right], \tag{30a}$$

$$n_1(s)=m_0(s)\left(\frac{c^*}{\kappa}\frac{\bar{c}^*c_T-K^{\mathrm{T}}}{c_T-c^*}\alpha+\beta^s\right). \tag{30b}$$

3.2.2. Solutions for Pore Pressure, Stresses, and Displacements under Deviatoric Loading. Considering Equation (18), the transforms to Equations (13), (14), and (17) while omitting the terms related to thermal effect result in the following equations in the Laplace transform domain:

$$\chi\frac{\tilde{\Xi}}{r}-\frac{1}{4}\frac{d\tilde{W}}{dr}+\frac{\alpha M}{2G}\frac{\tilde{Z}}{r}=0, \tag{31a}$$

$$\left(r^2\frac{d^2}{dr^2}+r\frac{d}{dr}-4\right)\tilde{W}=0, \tag{31b}$$

$$\left[r^2\frac{d^2}{dr^2}+r\frac{d}{dr}-\left(\frac{s}{c^*}r^2+4\right)\right]\tilde{Z}=0, \tag{31c}$$

in which $\chi=(1/2G)(\lambda+2G+\alpha^2M)$. Meanwhile, Equations (15) and (16) can degenerate to a nonhomogeneous linear differential equation set of order 2 with respect to constant coefficient.

$$\frac{d}{rdr}\left(r\tilde{U}_r^{(d)}\right)+2\frac{\tilde{U}_\theta^{(d)}}{r}=\tilde{\Xi}, \tag{32}$$

$$\frac{d}{rdr}\left(r\tilde{U}_\theta^{(d)}\right)+2\frac{\tilde{U}_r^{(d)}}{r}=\tilde{W}. \tag{33}$$

Noted that the solution regarding Equations (31a), (31b), and (31c)–(33) should remain to be bounded for vanishing $\tilde{Z}$, $\tilde{W}$, $\tilde{U}_r^{(d)}$, and $\tilde{U}_\theta^{(d)}$ at infinite boundaries.

After some manipulation, the solutions to displacement components, pore pressure, and stresses for deviatoric loading may be deduced from Equations (31a), (31b), and (31c)–(33) while considering the Laplace transformed boundary condition Equations (11a)–(11c).

$$\frac{2Gs\tilde{U}_r^{(d)}}{\sigma_d r_w}=\frac{C_1}{\beta}\left[K_1(\xi)+\frac{2}{\xi}K_2(\xi)\right]-C_2\frac{r_w}{2r}-C_3\left(\frac{r_w}{r}\right)^3 \tag{34a}$$

$$\frac{2Gs\tilde{U}_\theta^{(d)}}{\sigma_d r_w}=2\frac{C_1}{\beta^2}\frac{r_w}{r}K_2(\xi)+C_2\frac{1}{2\chi}\frac{r_w}{2r}-C_3\left(\frac{r_w}{r}\right)^3 \tag{34b}$$

$$-\frac{s\tilde{P}^{(d)}}{\sigma_d}=\frac{1-\nu}{1-2\nu}C_1K_2(\xi)+\frac{\alpha M}{4G\chi}C_2\left(\frac{r_w}{r}\right)^2 \tag{34c}$$

$$\frac{s\tilde{S}_r^{(d)}}{\sigma_d}=C_1\left[\frac{1}{\xi}K_1(\xi)+\frac{6}{\xi^2}K_2(\xi)\right]-\frac{1}{2(1-\psi)}C_2\left(\frac{r_w}{r}\right)^2-3C_3\left(\frac{r_w}{r}\right)^4 \tag{34d}$$

$$\frac{s\tilde{S}_{\theta}^{(d)}}{\sigma_d} = -C_1\left[\frac{1}{\xi}K_1(\xi) + \left(1 + \frac{6}{\xi^2}\right)K_2(\xi)\right] + 3C_3\left(\frac{r_w}{r}\right)^4 \tag{34e}$$

$$\frac{s\tilde{S}_{r\theta}^{(d)}}{\sigma_d} = 2C_1\left[\frac{1}{\xi}K_1(\xi) + \frac{3}{\xi^2}K_2(\xi)\right] - \frac{1}{4(1-\psi)}C_2\left(\frac{r_w}{r}\right)^2 - C_3\left(\frac{r_w}{r}\right)^4 \tag{34f}$$

where

$$C_1 = -\frac{4\beta(\psi - \nu)}{(D_2 - D_1)} \tag{35a}$$

$$C_2 = \frac{8(1-\psi)D_2}{D_2 - D_1}, \tag{35b}$$

$$C_3 = -\frac{\beta(D_2 + D_1) + 8(\psi - \nu)K_2(\beta)}{\beta(D_2 - D_1)} \tag{35c}$$

$$D_1 = 2(\psi - \nu)K_1(\beta) \tag{35d}$$

$$D_2 = \beta(1-\nu)K_2(\beta) \tag{35e}$$

with $\xi_3 = r\sqrt{s/c^*}$, $\beta_3 = r_w\sqrt{s/c^*}$, and $\psi = (1-\chi)/(1-2\chi)$.

When the relationship between shear strain and displacement defined by $\gamma_{r\theta} = (1/r)((\partial u_r/\partial\theta) + (\partial u_\theta/\partial r) - (u_\theta/r))$ and $\omega = (-1/r)((\partial u_r/\partial\theta) + (\partial/r\partial r)(ru_\theta))$ is adopted, it could be observed that the field variables in Equations ((29a)), ((29b)), ((29c)), ((34a)), ((34b)), ((34c)), ((34d)), ((34e)), and ((34f)) and the introduced transition variables in Equations (35a), (35b), (35c), (35d), and (35e) share the same fundamental expressions, excluding the negative sign appearing in the expressions of pore pressure compared to the one in the study of Detournay and Cheng [22]. The latter prescribes that the tension is positive. That is to say, the approach that Cui et al. [36] dealt with the whole variables with the negative sign to the corresponding formulas [37] is not appropriate.

The stress components in the time domain could be completed in favor of the numerical algorithm associated with the inversion technique for Laplace transforms offered by Stehfest [38], which has been adopted extensively in petroleum engineering.

Thus, the axial stress reads under plane strain condition

$$\tilde{\sigma}_z^{\mathrm{I}} = \nu\left(2\frac{\sigma_m}{s} + \tilde{\sigma}_r^{(a)} + \tilde{\sigma}_r^{(d)} + \tilde{\sigma}_\theta^{(a)} + \tilde{\sigma}_\theta^{(d)}\right) + (1-2\nu)\left[\alpha\left(\frac{p_0}{s} + \tilde{p}^{(a)} + \tilde{p}^{(d)}\right) + \beta^s\left(\frac{T_0}{s} + \tilde{T}^{(a)}\right)\right]. \tag{36}$$

3.3. Solution to the Elastic Uniaxial Stress Problem. This problem is purely elastic, and no time-dependent pore pressure and stresses are generated [35], and hence, the solution is only related to axial stress and reads as follows:

$$\sigma_z^{\mathrm{II}} = \sigma_v - 2\nu\sigma_m - (1-2\nu)(\alpha p_0 + \beta^s T_0). \tag{37}$$

Ultimately, the complete porothermoelastic solutions for stresses, pore pressure, and temperature around a pressurized vertical borehole are obtained on the condition that positive stress denotes compression

$$\sigma_r = \sigma_m + \sigma_d\cos 2\theta + \sigma_r^{(a)} + \sigma_r^{(d)}, \tag{38a}$$

$$\sigma_\theta = \sigma_m - \sigma_d\cos 2\theta + \sigma_\theta^{(a)} + \sigma_\theta^{(d)}, \tag{38b}$$

$$\sigma_z = \sigma_{zz}^{\mathrm{I}} + \sigma_{zz}^{\mathrm{II}}, \tag{38c}$$

$$\tau_{r\theta} = -\sigma_d\sin 2\theta + \sigma_{r\theta}^{(d)}, \tag{38d}$$

$$p = p_0 + p^{(a)} + p^{(d)}, \tag{38e}$$

$$T = T_0 + T^{(a)}. \tag{38f}$$

4. Numerical Results and Discussions

The input parameters for modeling results are listed in Table 1. Assign the temperature difference between mud T_m and formation T_0 to $\Delta T = 25\circ$C (heating) and $\Delta T = -25\circ$C (cooling), respectively.

4.1. Sensitivity Analysis. This subsection conducts the sensitivity analysis of remarkable influencing factors including thermal osmosis coefficient K^{T}, thermal diffusivity c_h, and permeability coefficient κ on induced pore pressure.

Figures 2 and 3 show the induced pore pressure distributions where porothermoelastic osmosis solution, porothermoelastic, and pure poroelastic models occur at 10^{-4}day.

The undrained loading effect reflects the short-term behavior of low-permeability rock and is induced by deviatoric stress [24, 25]. For the pure poroelastic model [24] (see Figure 3(c)), the undrained loading effect does increase the pore pressure in regions near the wellbore wall.

As shown from Figure 2(a), in line with the common porothermoelastic (THM) model [11], heating the wellbore generates an increased pore pressure in regions near the borehole wall for smaller time intervals $t = 10^{-4}$day, since the thermal expansion of fluid is higher than that of the solid skeleton but the extremely low permeability of rock restricts the excess pore pressure to immediately dissipate. However, the present results suggest that heating (negative temperature gradient $\Delta T < 0$) does not always further guarantee a pore pressure building up. The reduced pore pressure associated with porothermoelastic osmosis (THMO) solution is attributed to the weakened phenomenon of the undrained loading effect by the thermal osmosis effect. This weaken phenomenon occurs where the thermal osmotic coefficient K^{T} is significantly large, and signs of K^{T} and temperature gradient ΔT share the opposite form, for example, $K^{\mathrm{T}} > 0$ and $\Delta T < 0$. This special case produces a backflow to pull the fluid out of formation and even exceedingly dehydrates rock [8]. Naturally, the lower pore pressure fortifies the effective stresses and then increases the rock strength to failure and therefore culminates in better condition to stabilize wellbore.

Table 1: List of input data ([8, 11, 39]).

Parameters	Value	Units
In situ conditions		
Overburden stress (σ_v)	29	kPa/m
Maximum horizontal in situ stress (σ_H)	25	kPa/m
Minimum horizontal in situ stress (σ_h)	20	kPa/m
Formation pore pressure (p_0)	9.8	kPa/m
Wellbore conditions		
Well depth (true vertical depth)	1000	m
Wellbore radius (r_w)	0.1	m
Formation pore pressure (p_w)	12	kPa/m
Material parameters		
Elastic modulus (E)	9.474	GPa
Possion's ratio (ν)	0.24	
Grain bulk modulus (K_s)	27.5	GPa
Grain bulk modulus (K_f)	2.15	GPa
Permeability coefficient (κ)	5.0×10^{-9}, 5.0×10^{-10}, 5.0×10^{-11}	$m^2/(MPa \cdot s)$
Reference porosity (ϕ)	0.14	
Linear expansion coefficient for solid skeleton (α^s)	6.0×10^{-6}	1/K
Volumetric expansion coefficient for pore fluid (α^f)	3.0×10^{-4}	1/K
Thermal diffusivity (c_h)	$7.15 \times 10^{-7}/1.6 \times 10^{-6}$	m^2/s
Thermal osmotic coefficient (K_T)	1×10^{-10}, 1×10^{-11}, 1×10^{-12}, 1×10^{-13}	$m^2/(s \cdot K)$
Cohesion of rock (C)	10	MPa
Internal friction angle (φ)	20	Degree

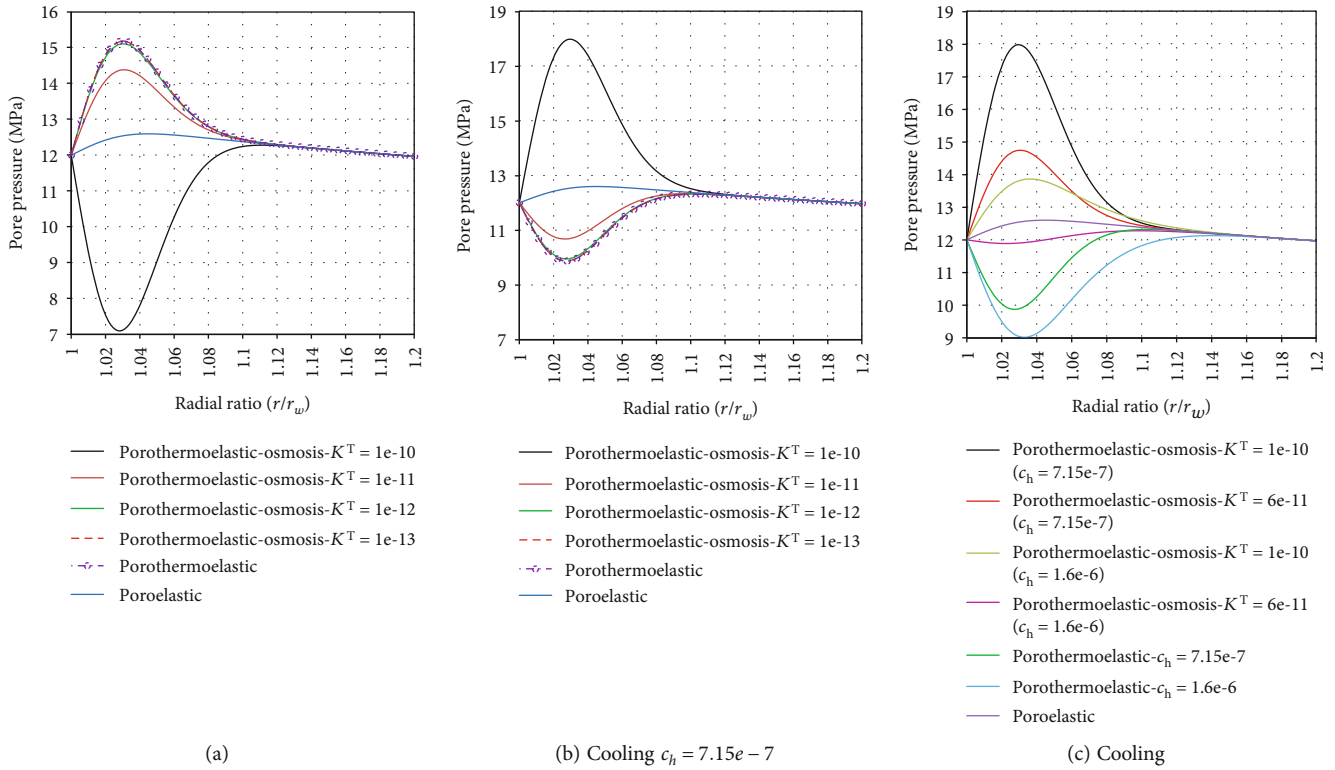

(a) (b) Cooling $c_h = 7.15e-7$ (c) Cooling

Figure 2: Induced pore pressure varying with r/r_w at $\theta = 90\circ$ wherein different conditions are prescribed.

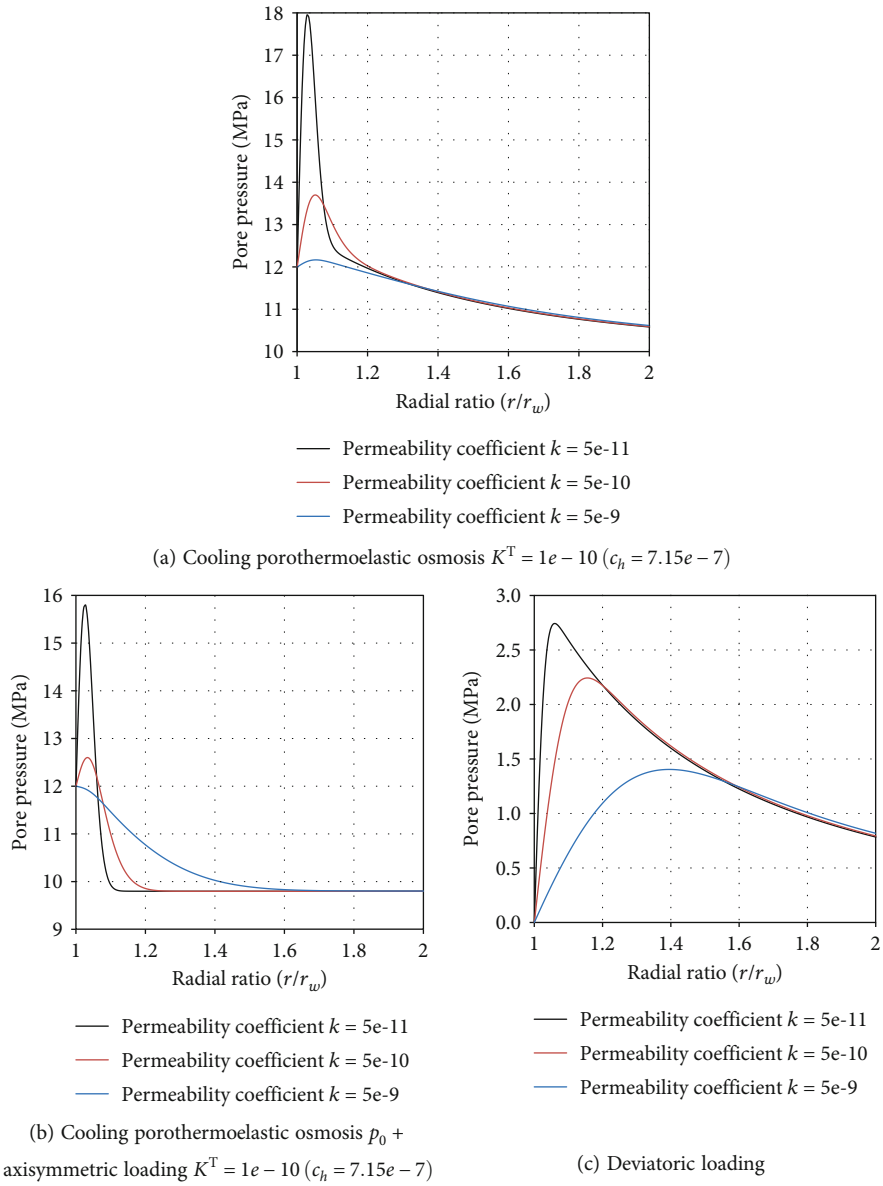

(a) Cooling porothermoelastic osmosis $K^{\mathrm{T}} = 1e-10$ ($c_h = 7.15e-7$)

(b) Cooling porothermoelastic osmosis p_0 + axisymmetric loading $K^{\mathrm{T}} = 1e-10$ ($c_h = 7.15e-7$)

(c) Deviatoric loading

Figure 3: Induced pore pressure varying with r/r_w at $\theta = 90\circ$ wherein different permeability coefficients are prescribed.

The intensifying case (see Figure 2(b)) is stipulated as the same sign for cooling (positive temperature gradient $\Delta T > 0$) and the significantly large thermal osmosis coefficient $K^{\mathrm{T}} > 0$. The intensifying case causes drilling fluid water in mud to flow into the formation. The increased pore pressure associated with this intensifying case reduces effective stresses and thus decreases the rock strength to failure. It deteriorates the wellbore stability. The previous investigator, i.e., Ghassemi and Diek [8], likewise testified the similar view that the thermal osmosis effect enhances or reduces the chemical osmosis effect that rests upon the sign between thermal osmotic coefficient and temperature gradient, and the magnitude of thermal osmotic coefficient as well. Besides, in the case of a considerably small thermal osmosis coefficient, the induced pore pressures share the approximatively identical significance compared THMO model with the THM one. Therefore, it is appropriate for neglecting the thermal osmosis effect.

When the same thermal osmotic coefficient is prescribed, the thermal osmosis effect enhancing the undrained loading effect is more significant for the rock characterized by the less value that of thermal diffusivity c_h (see Figure 2(c)). Also, the case of larger value that of thermal diffusivity and lower thermal osmotic coefficient would turn to the reduction of the undrained loading effect and further decrease pore pressure. Moreover, the thermal osmosis effect with a larger thermal osmotic coefficient is more vulnerable to undertake the role to enhance the undrained loading effect, when the same thermal diffusivity is stipulated.

With the THMO model considering the cooling effect, the total pore pressure as presented in Figure 3(a) equals the superposition of the original formation pore pressure and axisymmetric loading effect (see Figure 3(b)) and deviatoric loading (see Figure 3(c)). The thermal osmosis effect on the pore pressure is reduced in the case of a larger

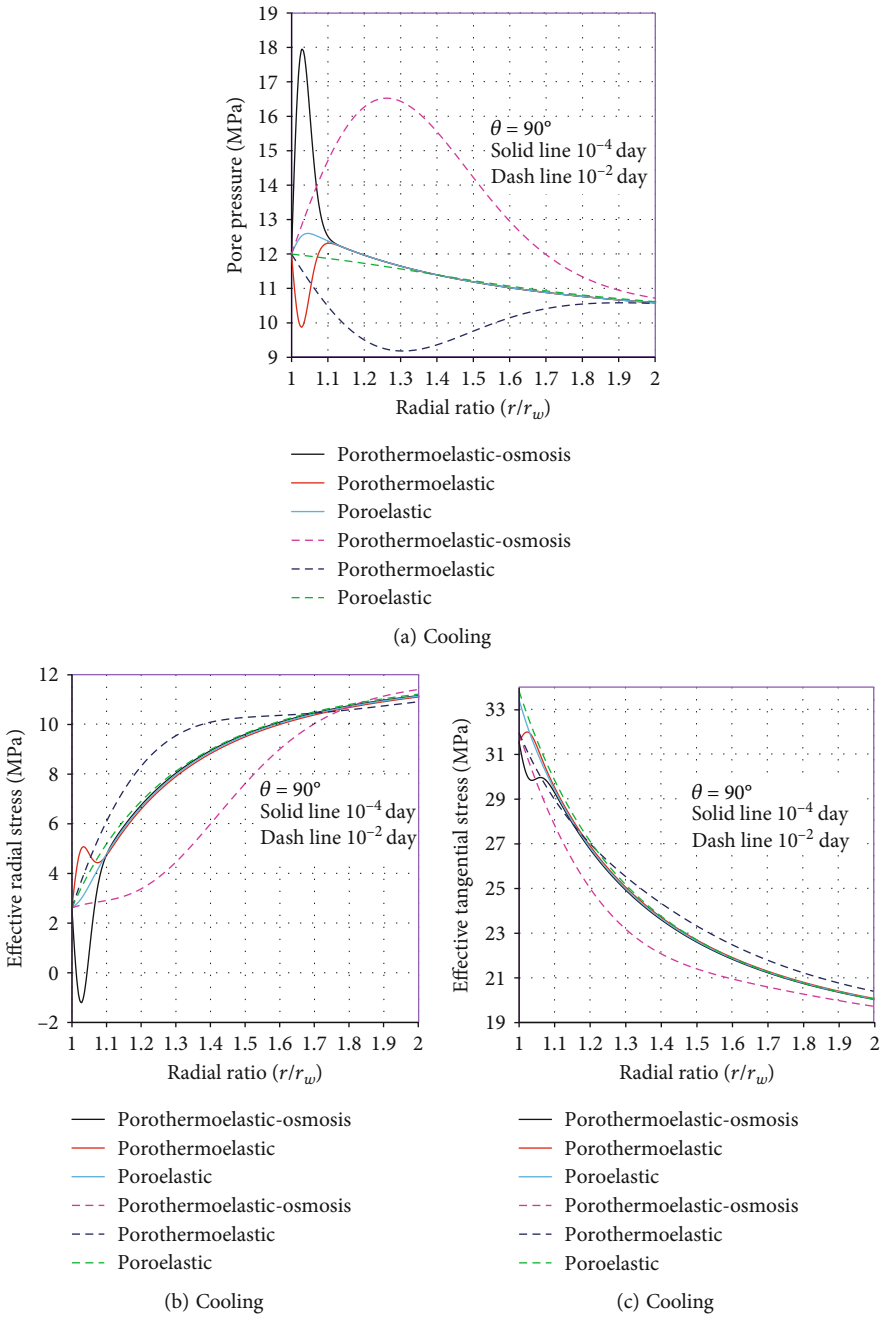

Figure 4: Induced pore pressure and effective stresses varying with r/r_w at $\theta = 90\circ$ wherein different conditions are prescribed.

permeability coefficient κ. On the contrary, the cases of lower magnitudes of permeability coefficient intensify the thermal osmosis effect to generate the more distinct backflow phenomenon, so that the undrained loading effect is reduced and consequently the pore pressure drops.

4.2. Time Dependence of the Induced Pore Pressure and Effective Total Stresses. Figure 4 evaluates the induced pore pressure and effective stress profiles at different times when the THMO model and THM case where cooling and the pure poroelastic one are examined.

Figure 4 describes the induced pore pressure and effective total stresses including radial and tangential profiles (porothermoelastic osmosis solution, $c^h = 7.15 * 10^{-7}$, $K^T = 1 * 10^{-10}$; porothermoelastic model, $c^h = 7.15 \times 10^{-7}$) and pure poroelastic model when wellbore is subjected to cooling or isothermal condition, respectively, at different times.

When the thermal osmosis effect intensifies the undrained loading effect, the thermally induced pore pressure and effective stresses including radial and tangential stresses of THMO model behave the opposite variation compared to the common THM one. Higher pore pressure leads to effective tensile radial stress and consequently produces the probability for borehole spalling inside the formation (or outburst) [40, 41] at smaller time interval after drilling a borehole (see Figure 4(b)). However, the

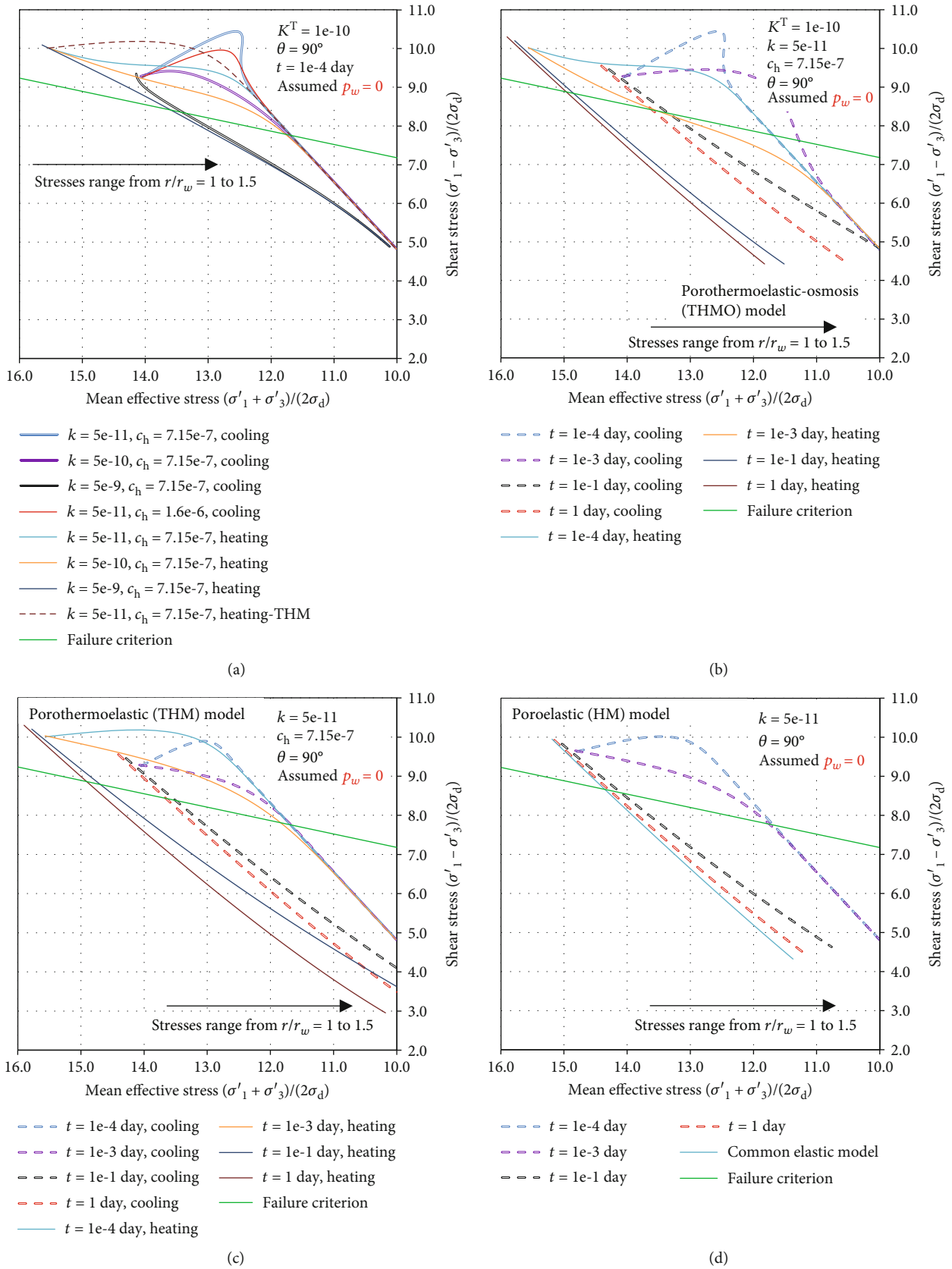

Figure 5: The time-dependent shear failure potentials against different models including porothermoelastic osmosis (THMO), porothermoelastic (THM), and pure poroelastic (HM).

values of pore pressure gradually shift inward the formation with diminishing magnitudes as time progress. This case also reduces effective stresses, and the shear failure zones are displaced into formation in nature. The more compressive effective radial stress which the regions of tensile spalling failure disappear can be observed at a later time. The cooling effect naturally reduces the stress as presented in the constitutive Equation (1); therefore, Figure 4(c) shows the pure poroelastic (HM) model has larger effective tangential stress than that of THMO and THM ones, especially the regions at or very close to the borehole wall. But, the increased pore pressure due to the thermal osmosis effect further reduces the magnitude of tangential stress near the borehole wall.

As time elapses, the common THM one indicates that the reduction and less minimum magnitude of pore pressure is a reverse analogy to that of the THMO solution and pure poroelastic model near the borehole wall region. Finally, the reduced shear stress in the form of a difference between effective tangential stress and effective radial stress stabilizes the wellbore with regard to shear failure in regions near the wellbore wall.

4.3. Time-Dependent Potential of Borehole Collapse. One illustrates the potential of borehole collapse for vertical borehole against different models in this subsection.

Mohr-Coulomb strength criterion is used to study the borehole stability. It is commonly expressed in terms of the shear stress $(\sigma_1' - \sigma_3')/2$ and mean effective stress $(\sigma_1' + \sigma_3')/2$ (the effective stress is defined by $\sigma_{ij}' = \sigma_{ij} - \alpha p \delta_{ij}$) to predict the failure of a geotechnical material [42].

$$\left(\frac{\sigma_1' - \sigma_3'}{2}\right) = C\cos\varphi + \left(\frac{\sigma_1' + \sigma_3'}{2}\right)\sin\varphi, \tag{39}$$

where C and φ, respectively, correspond to the intrinsic cohesive strength and internal friction angle of the rock. Besides, the abovementioned maximum and minimum principal stresses σ_1' and σ_3' correspond to the eigenvalues σ_n of the matrix of the effective stress tensor $(\sigma_{ij}',\ i, j \in (r, \theta, z))$ in Equations (34a)–(34f) around the borehole. One obtains the two principal stresses by solving the following characteristic equation:

$$\begin{vmatrix} \sigma_r' - \sigma_n & \tau_{r\theta} & \tau_{rz} \\ \tau_{r\theta} & \sigma_\theta' - \sigma_n & \tau_{\theta z} \\ \tau_{rz} & \tau_{\theta z} & \sigma_{zz}' - \sigma_n \end{vmatrix} = 0. \tag{40}$$

Note that a profile above the failure envelope implies failure.

On the whole, Figure 5 shows the borehole collapse related to the three aforementioned models is time-dependent. The locations of borehole collapse occur inside the formation (or next to the borehole wall) at an earlier time but are displaced at the borehole wall at a later time. The combination of effective compressive tangential stress and effective tensile radial stress renders the maximum magnitude of the shear stress $(\sigma_1' - \sigma_3')/2$ to occur inside the formation. Noted that the shear stress $\tau_{r\theta}$ of a vertical borehole appropriately has zero magnitudes at the borehole wall or the formation; thus, the effective maximum or minimum principal stress σ_1' and σ_3' can practically equal to the effective tangential stress and effective radial stress. The potential of borehole collapse occurring at the borehole wall increases with increasing time; this is because maximum effective tangential stress occurs at the borehole at a later time.

With the cooling cases considered, Figure 5(a) shows that the obvious thermal osmosis effect further enhances the undrained effect for lower permeability rock at a given thermal diffusion coefficient, and thus, the risk of borehole collapse increases and the failure location occurs inside the formation. Similarly, the strengthening effect of the thermal osmosis effect on the undrained effect for lower permeability rock corresponds to the rock with a smaller thermal diffusion coefficient at a given permeability coefficient. The cooling effect reduces the effective tangential stress, and thus, the mean effective stresses of the cooling cases are smaller than those of the heating cases. The potential of borehole collapse firstly occurs at the borehole wall for heating cases of the THMO model in Figure 5(a), but the location of borehole collapse could appear inside the formation for the THM model at a given earlier time. This is because the thermal osmosis effect reduces the undrained effect and renders the pore pressure to decrease, and thus, the effective compressive radial stress along the radial distance eliminates the possibility of the maximum shear stress occurring inside the formation.

With the case of the thermal osmosis effect strengthening the undrained effect considered, Figure 5(b) again confirms the view that the locations of borehole collapse occur inside the formation at an earlier time when the drilling mud cools the formation. However, Figure 5(c) indicates the aforementioned phenomenon corresponds to the heating borehole. The heat effect further increases the risk of borehole collapse compared to Figures 5(c) and 5(d). Also, Figure 5(d) shows the time-dependent effect disappears with increasing time and approaches the elastic case.

This study presents the effect of thermal osmosis effect on wellbore stability and can also be introduced to the discussion of thermal osmosis effect on hydraulic fracturing [43, 44].

5. Conclusions

Under plane strain condition, the present paper formulates a set of porothermoelastic analytical solutions of the vertical wellbore drilled through an isotropic porous rock formation subjected to thermal osmosis effect and nonhydrostatic remote stress.

(1) When a lower permeability rock is characterized by the substantially large thermal osmotic coefficient and the smaller thermal diffusivity, the thermal osmosis effect more significantly intensifies or weakens the undrained loading effect (poroelastic effect), and it is not appropriate for neglecting this effect

(2) In the case of the positive magnitude of the product of the significantly large thermal osmotic coefficient

and temperature gradient, the thermal osmosis effect intensifies the undrained loading effect and leads to a build-up of pore pressure. Accordingly, lower effective stresses increase the mean shear stress and tend to deteriorate wellbore stability. The weakening cases, on the contrary, can stabilize wellbore with respect to shear failure

(3) The predrilling mud-weight design is suggested to consider the time-dependent locations of borehole collapse since the locations firstly occur inside the formation, whereas it is displaced at the borehole wall

Data Availability

The reader can request the data by contacting the corresponding author.

Conflicts of Interest

The authors declare that they have no conflicts of interest.

Acknowledgments

This research is supported by the Research and demonstration of drilling and completion technology for extended reach wells exceeding 6000 meters in Laizhou Bay (No. CNOOC-KJ135ZDXM36TJ06TJGD202201).

References

[1] P. T. Delaney, "Rapid intrusion of magma into wet rock: groundwater flow due to pore pressure increases," *Journal of Geophysical Research B*, vol. 87, no. B9, pp. 7739–7756, 1982.

[2] D. F. McTigue, "Thermoelastic response of fluid-saturated porous rock," *Journal of Geophysical Research-Solid Earth*, vol. 91, no. B9, pp. 9533–9542, 1986.

[3] D. F. McTigue, "Flow to a heated borehole in porous, thermoelastic rock: analysis," *Water Resources Research*, vol. 26, no. 8, pp. 1763–1774, 1990.

[4] Y. Wang and E. Papamichos, "Conductive heat flow and thermally induced fluid flow around a well bore in a poroelastic medium," *Water Resources Research*, vol. 30, no. 12, pp. 3375–3384, 1994.

[5] X. Li, L. Cui, and J. C. Roegiers, "Thermoporoelastic analyses of inclined boreholes," in *Paper presented at the SPE/ISRM Rock Mechanics in Petroleum Engineering*, pp. 1–9, Trondheim, Norway, 1998.

[6] Y. Zhou, R. Rajapakse, and J. Graham, "Coupled consolidation of a porous medium with a cylindrical or a spherical cavity," *International Journal for Numerical and Analytical Methods in Geomechanics*, vol. 22, no. 6, pp. 449–475, 1998.

[7] Y. Zhou, R. Rajapakse, and J. Graham, "A coupled thermoporoelastic model with thermo-osmosis and thermal-filtration," *International Journal of Solids and Structures*, vol. 35, no. 34-35, pp. 4659–4683, 1998.

[8] A. Ghassemi and A. Diek, "Porothermoelasticity for swelling shales," *Journal of Petroleum Science and Engineering*, vol. 34, no. 1-4, pp. 123–135, 2002.

[9] Y. Wang and M. B. Dusseault, "A coupled conductive-convective thermo-poroelastic solution and implications for wellbore stability," *Journal of Petroleum Science and Engineering*, vol. 38, no. 3-4, pp. 187–198, 2003.

[10] G. Chen and R. T. Ewy, "Thermoporoelastic effect on wellbore stability," *SPE Journal*, vol. 10, no. 2, pp. 121–129, 2005.

[11] Y. Abousleiman and S. Ekbote, "Solutions for the inclined borehole in a porothermoelastic transversely isotropic medium," *Journal of Applied Mechanics*, vol. 72, no. 1, pp. 102–114, 2005.

[12] H. S. Farahani, M. Yu, S. Miska, N. Takach, and G. Chen, "Modeling transient thermo-poroelastic effects on 3D wellbore stability," in *Paper presented at the SPE Annual Technical Conference and Exhibition*, pp. 1–12, San Antonio, Texas, USA, 2006.

[13] Q. Tao and A. Ghassemi, "Poro-thermoelastic borehole stress analysis for determination of the in situ stress and rock strength," *Geothermics*, vol. 39, no. 3, pp. 250–259, 2010.

[14] B. Wu, X. Zhang, R. G. Jeffrey, and B. Wu, "A semi-analytic solution of a wellbore in a non-isothermal low-permeability porous medium under non-hydrostatic stresses," *International Journal of Solids and Structures*, vol. 49, no. 13, pp. 1472–1484, 2012.

[15] M. Gomar, I. Goodarznia, and S. R. Shadizadeh, "Transient thermo-poroelastic finite element analysis of borehole breakouts," *International Journal of Rock Mechanics and Mining Sciences*, vol. 71, pp. 418–428, 2014.

[16] M. F. Kanfar, Z. Chen, and S. S. Rahman, "Fully coupled 3D anisotropic conductive-convective porothermoelasticity modeling for inclined boreholes," *Geothermics*, vol. 61, pp. 135–148, 2016.

[17] Z. Q. Fan and R. Parashar, "Analytical solutions for a wellbore subjected to a non-isothermal fluid flux: implications for optimizing injection rates, fracture reactivation, and EGS hydraulic stimulation," *Rock Mechanics and Rock Engineering*, vol. 52, no. 11, pp. 4715–4729, 2019.

[18] Z. Q. Fan, R. Parashar, and Z. H. Jin, "Impact of convective cooling on pore pressure and stresses around a borehole subjected to a constant flux: implications for hydraulic tests in an enhanced geothermal system reservoir," *Interpretation*, vol. 8, no. 2, pp. SG13–SG20, 2020.

[19] J. Gao, J. Deng, K. Lan, Z. Song, Y. Feng, and L. Chang, "A porothermoelastic solution for the inclined borehole in a transversely isotropic medium subjected to thermal osmosis and thermal filtration effects," *Geothermics*, vol. 67, pp. 114–134, 2017.

[20] Z. Song, F. Liang, and S. Chen, "Thermo-osmosis and mechano-caloric couplings on THM responses of porous medium under point heat source," *Computers and Geotechnics*, vol. 112, pp. 93–103, 2019.

[21] Z. Song, Y. Hao, and H. Liu, "Analytical study of the thermo-osmosis effect in porothermoelastic responses of saturated porous media under axisymmetric thermal loadings," *Computers and Geotechnics*, vol. 123, article 103576, 2020.

[22] X. Zhai and K. Atefi-Monfared, "Explanation of early failure in porous media confined with flexible layers, considering thermo-osmosis, thermal-filtration and heat sink from fluid dilation," *Computers and Geotechnics*, vol. 122, article 103501, 2020.

[23] J. J. Gao, H. Lin, B. S. Wu, J. Deng, and H. Liu, "Porochemothermoelastic solutions considering fully coupled thermo-

hydro-mechanical-chemical processes to analyze the stability of inclined boreholes in chemically active porous media," *Computers and Geotechnics*, vol. 134, article 104019, 2021.

[24] E. Detournay and A. H. D. Cheng, "Poroelastic response of a borehole in a non-hydrostatic stress field," *International Journal of Rock Mechanics and Mining Science and Geomechanics Abstracts*, vol. 25, no. 3, pp. 171–182, 1988.

[25] G. Chen and R. T. Ewy, "Investigation of the undrained loading effect and chemical effect on shale stability," in *Paper presented at the SPE/ISRM Rock Mechanics Conference*, Irving, Texas, 2002.

[26] C. Dirksen, "Thermo-osmosis through compacted saturated clay membranes," *Soil Science Society of America Journal*, vol. 33, no. 6, pp. 821–826, 1969.

[27] D. H. Gray, *Coupled Flow Phenomena in Clay-Water Systems*, University of Michigan, 1966.

[28] C. L. Carnahan, "Thermodynamic coupling of heat and matter flows in near-field regions of nuclear waste repositories," *MRS Online Proceedings Library*, vol. 26, pp. 1023–1030, 1983.

[29] S. T. Horseman and T. J. McEwen, "Thermal constraints on disposal of heat-emitting waste in argillaceous rocks," *Engineering Geology*, vol. 41, no. 1-4, pp. 5–16, 1996.

[30] J. M. Soler, "The effect of coupled transport phenomena in the Opalinus Clay and implications for radionuclide transport," *Journal of Contaminant Hydrology*, vol. 53, no. 1-2, pp. 63–84, 2001.

[31] J. Gonçalvès and J. Trémosa, "Estimating thermo-osmotic coefficients in clay-rocks: I. Theoretical insights," *Journal of Colloid and Interface Science*, vol. 342, no. 1, pp. 166–174, 2010.

[32] E. Detournay and A. H. D. Cheng, "Fundamentals of poroelasticity," in *Analysis and Design Methods*, pp. 113–171, Elsevier, 1993.

[33] R. W. Zimmerman, "Coupling in poroelasticity and thermoelasticity," *International Journal of Rock Mechanics and Mining Sciences*, vol. 37, no. 1-2, pp. 79–87, 2000.

[34] Y. Abousleiman and L. Cui, "Poroelastic solutions in transversely isotropic media for wellbore and cylinder," *International Journal of Solids and Structures*, vol. 35, no. 34-35, pp. 4905–4929, 1998.

[35] J. P. Carter and J. R. Booker, "Elastic consolidation around a deep circular tunnel," *International Journal of Solids and Structures*, vol. 18, no. 12, pp. 1059–1074, 1982.

[36] L. Cui, Y. Abousleiman, A. H. D. Cheng, and J. C. Roegiers, "Time-dependent failure analysis of inclined boreholes in fluid-saturated formations," *Journal of Energy Resources Technology*, vol. 121, no. 1, pp. 31–39, 1999.

[37] L. Cui, A. H. D. Cheng, and Y. Abousleiman, "Poroelastic solution for an inclined borehole," *Journal of Applied Mechanics*, vol. 64, no. 1, pp. 32–38, 1997.

[38] H. Stehfest, "Algorithm 368: numerical inversion of Laplace transforms [D5]," *Communications of the ACM*, vol. 13, no. 1, pp. 47–49, 1970.

[39] http://www.pmi.ou.edu/images/Pbore%20pics/criticalregionwithbedding.jpg.

[40] L. Paterson, "A model for outbursts in coal," *International Journal of Rock Mechanics and Mining Science and Geomechanics Abstracts*, vol. 23, no. 4, pp. 327–332, 1986.

[41] A. H.-D. Cheng, Y. Abousleiman, and J. C. Roegiers, "Review of some poroelastic effects in rock mechanics," *International Journal of Rock Mechanics and Mining Science and Geomechanics Abstracts*, vol. 30, no. 7, pp. 1119–1126, 1993.

[42] J. C. Jaeger, N. G. W. Cook, and R. W. Zimmerman, *Fundamentals of Rock Mechanics*, John Wiley & Sons, 4rd ed. edition, 2007.

[43] Y. Wang, B. Hou, D. Wang, and Z. Jia, "Features of fracture height propagation in cross-layer fracturing of shale oil reservoirs," *Petroleum Exploration and Development*, vol. 48, no. 2, pp. 469–479, 2021.

[44] B. Hou, Y. F. Dai, C. L. Zhou, K. Zhang, and F. Liu, "Mechanism study on steering acid fracture initiation and propagation under different engineering geological conditions," *Geomechanics and Geophysics for Geo-Energy and Geo-Resources*, vol. 7, no. 3, pp. 1–14, 2021.